Numerical heterodyne holography with two-dimensional photodetector arrays

F. Le Clerc, L. Collot

Thomson CSF Optronique, Rue Guynemer B.P. 55,
78 283 Guyancourt, France

M. Gross

Laboratoire Kastler-Brossel, UMR 8552 CNRS,
Ecole Normale Supérieure,
Université Pierre et Marie Curie,
24 rue Lhomond 75231 Paris cedex 05 France

We present an original heterodyne holography method for digital holography that relies on two-dimensional heterodyne detection to record the phase and the amplitude of a field. The technique has been tested on objects as much as 13 mm in size. Consistency checks were performed, and high-resolution images were computed. We show the requirement for a spatial filter to select properly sampled near-axis photons. Heterodyne holography is superior to off-axis digital holography for both field of view and resolution.

As was demonstrated by Gabor[1], in the early 1950.s, the purpose of holography is to record the phase and the amplitude of the light coming from an object under coherent illumination. Classical holography does not provide straightforward access to the holographic data. For quantitative analyses of those data, in digital holography[2] (DH) photographic films were replaced by two-dimensional electronic detectors. In both digital and thin-film holograms a ghost field and the remaining part of the reference field are superimposed upon the reconstructed object field[3]. A solution to this problem is to tilt the reference beam with respect to the object[4], to separate physically the spatial-frequency components. Although this off-axis technique is acceptable for high-resolution holographic films, it is hardly compatible with the limited resolution of digital holograms. All these artifacts arise from the fact that among all these methods only one field quadrature is measured. Measuring both quadratures requires recording at least two interferograms with distinct reference phases[5]. In classical holography this is done with a thick plate that records several intensity fringes in depth.

In this Letter we describe a heterodyne holographic scheme in which the reference beam is dynamically phase shifted with respect to the signal field. This shift produces time-varying interferograms on a two-dimensional sensor. In our experiment the phase shift is linear in time (frequency shift). Intensity I in the detector plane results from the interference of the signal field with the δf-shifted reference field:

$$I(t) = |E_S + E_R \exp(2i\pi\delta f t)|^2 \qquad (1)$$

where E_S and E_R represent the complex amplitudes of the signal and the reference fields, respectively. L intensity I_l $(l = 0...L-1)$ measurements are performed within a δf period at $t_l = 2\pi l/\delta f$. We obtain E_S by demodulating I :

$$E_S = \left(\frac{1}{LE_R^*}\right) \sum_{l=0}^{L-1} I_l \exp i\left(\frac{2\pi l}{L}\right) \qquad (2)$$

where * is the complex conjugate. For $L = 4$, E_S is proportional to $(I_0 - I_2) + i(I_1 - I_3)$. Heterodyne holography (HH) thus measures the phase, using the information obtained at different times, and DH extracts the phase from measurements made of different pixels[6]. In both cases the sampling theorem[2] restricts the largest admissible field-of-view angle θ to

$$|\theta| \le \theta_{max} = \lambda/(2d_{pixel}) \qquad (3)$$

where λ is the wavelength and d_{pixel} is the pixel spacing. In DH the object must be off axis, which yields the constraint [3] that $\theta \ge \theta_{min} = Nd_{pixel}/(2D)$, where N is the number of pixels and D is the sensor-to-object distance. The DH field of view, $\theta_{min} \le \theta\theta_{max}$, is thus much smaller than for HH: $|\theta| \le \theta_{max}$. Whereas $\theta_{min} \le \theta_{max}$. restricts DH to the far field with respect to $D_{min} = Nd_{pixel}/\lambda$, HH works in both the near field and the far field modes. In the far field, both HH and DH angular resolution reaches the diffraction limit, $\theta_{diff} = \lambda/(Nd_{pixel})$, which corresponds to the two dimensional sensor's size. In HH the number of resolved pixels (i.e., field of view/angular resolution) is N. This remains true in the near-field regime.

Although HH works on ref lection, we focus here on a transmission configuration. The general setup, shown
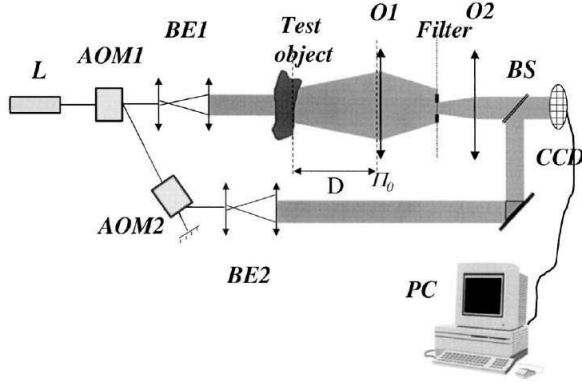
Fig. 1. Experimental setup: L, He.Ne laser; other abbreviations defined in text.
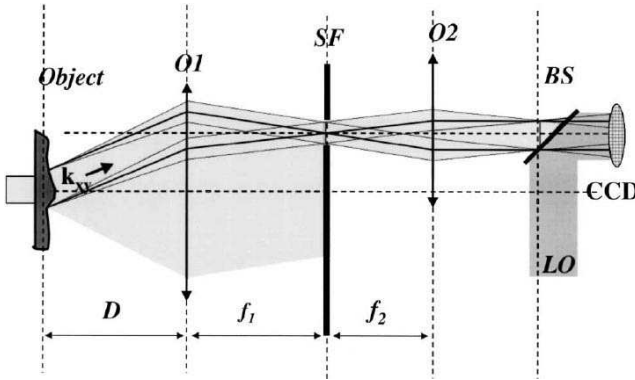

Fig. 2. SF system: LO, local oscillator; other abbreviations defined in text.

in Fig. 1, is a Mach.Zehnder interferometer composed of two beams (reference and signal) from the same coherent source (a 5-mW He.Ne laser). The two beams are expanded by beam expanders BE1 and BE2 and combined by a beam splitter (BS) on a CCD camera with $N_x = 768$ and $N_y = 576$ pixels, $d_{pixel_x} = 8.6$ μm and $d_{pixel_y} = 8.3$ μm. All x and y subscripts below refer to x or y axes, respectively. We δf shift the reference beam by combining two acousto-optic modulators, AOM1 and AOM2, working at $\Delta f + \delta f$ and $-\Delta f$, respectively, with $\Delta f = 80$ MHz. $\delta f = 6.25$ Hz is equal to one quarter of the CCD image frequency $f_I = 25$ Hz ($L = 4$). The video frame is acquired by an 8-bit analog frame grabber (Matrox Meteor), and a Pentium II 450-MHz computer calculates the complex field in real time.

To select the signal on-axis photons, we insert between the object and the BS a spatial filter system (Fig. 2) composed of two confocal objectives, O1 (focal length, $f_1 = 50$ mm) and O2 ($f_2 = 25$ mm), with a spatial filter (SF) in their common focal plane. O1 transforms the field into its k-space components in its focal plane where the SF selects the photons that fulfill Eq.3. O2

backtransforms the field to real space. The SF, O2, the BS, and the CCD are kept in alignment, so the selected photons reach the CCD nearly parallel to the reference beam. Equation 3 yields a rectangular SF of dimensions $d_{x,y} = 2\tan(\lambda/2d_{pixel_{x,y}})f_2$ ($d_x = 1.84$ mm and $d_y = 1.90$ mm). The O1-O2 optical system magnifies the incoming beam by a factor $f_1/f_2 = 1/2$. Our setup thus has x and y fields of view of $\pm 1.05°$ and $\pm 1.09°$, corresponding to an equivalent CCD with magnified pixels $d'_{pixel} = 2d_{pixel}$. O1 is fixed, and the SF, O2, the BS, and the CCD camera can be x and y translated by step motors. When the SF is not centered on the optical axis of O1, the system records holograms that correspond to tilted k components, as depicted in Fig. 2. Those displacements allow us to center the SF accurately. This feature will be used in the future to record wider-field-of-view holograms by merging several holograms with different k-component tilts.

To test our setup quantitatively, we recorded the hologram of a narrow slit 9.5 mm high and $w = 35\mu$m wide at $D = 60$ cm with a 480-ms integration time. We got $E_S(x, y, z = 0)$ on the equivalent CCD. To compute $E_S(x, y, z = D)$ on the slit we considered the Fresnel propagation of E_S from $z = 0$ to $z = D$, which can be formally expressed as an x and y convolution product (symbol $\otimes$):

$$E_S(x,y,D) = e^{ik_0 D}\left[P(z = D) \otimes E_S(x,y,0)\right]$$
$$P(x,y,z) = \frac{1}{i\lambda z}\exp\left[i\frac{k_0}{2z}\left(x^2 + y^2\right)\right] \tag{4}$$

We obtained a 13.2 mm × 9.6 mm (equivalent CCD size) contact image of the slit in its plane [Fig. 3(a)]. The $z = 0$ field is calculated on a 1024 × 1024 grid by bilinear interpolation of the 768 × 576 experimental points, and the convolution product is calculated by the fast-Fourier-transformmethod[5], with the grid size kept constant over z. Figure 3(b) shows the intensity along the AA' cut. Points are experimental data on the fast-Fourier-transform grid. The solid curve is the calculated diffracted intensity of an ideal wide slit (dashed lines). Both diffraction and spatial averaging over the magnified pixels are calculated; the agreement is good. D is larger than $D_{min_x} = 35.9$ cm and $D_{min_y} = 25.0$ cm, so diffraction is the main contributor to resolution; here it is assumed to be equal to the distance that yields a sharp contact imaging. Comparing D with the O1-to-object distance, we find that the equivalent CCD is located ~ 27 cm behind O1. This location does not depend on D and agrees with the positions of O1, O2, and the CCD.

Figure 4 shows the contact image of a transmission U.S. Air Force test chart target at $D = 58$ cm. At the right, Fig. 4 is exactly on focus, whereas at the left the target is 1.2 mm out of focus. The blur is due to a defocus equal to the x depth of focus (DOF): $DOF_{x,y} = \lambda(1 - NA_{x,y}^2)^2/NA_{x,y}^2)^2$ ($DOF_x = 1.22$ mm, $DOF_x = 2.32$ mm). Here $NA_{x,y} = N_{x,y}d'_{pixel_{x,y}}/D$ is the numerical aperture.
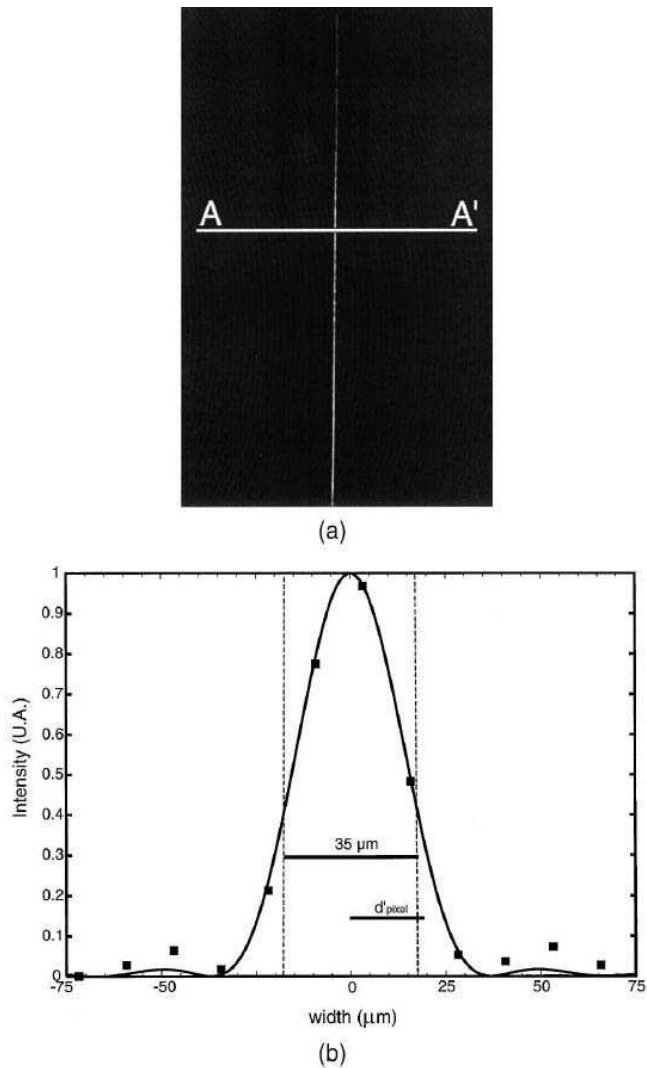
(a)

(b)

Fig. 3. (a) Contact image of the slit (b) cut along AA': filled squares, experimental intensity points; dashed lines, initial slit; solid curve, theoretical intensity profile.
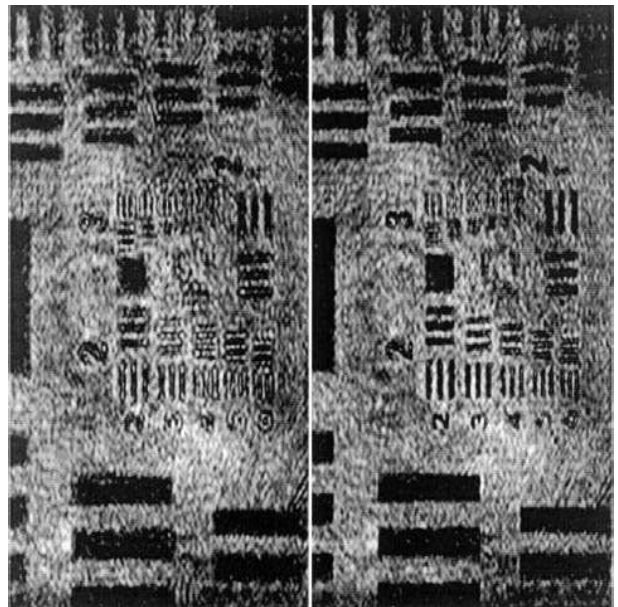

Fig. 4. Contact image of a U.S. Air Force test chart target at $D = 58$ cm. Right, image on focus; left, 1.2-mm out-of-focus image.

cause it detects amplitude. The time-varying character of HH provides good immunity against any dc and non-harmonic (with respect to δf) errors. The CCD image phase shift (90°) is highly accurate because it results from a frequency-offset δf. It is also possible to shift the heterodyne frequency δf for sideband heterodyne detection. Making $\delta f = (1/4)f_I + f_{mod}$ allows the vibration of an object at f_{mod} to be detected. HH works with a low-power cw laser. HH may be performed with low coherent laser sources to select a narrow space slice on the object where coherence is conserved.

Within the numerous possible applications of the method, we have explored diffusing media[7] and aperture synthesis applications, and further experiments are in progress. In both cases, a SF is useful.

Figure 5 shows the central part of the contact images of black characters printed on a diffusive plastic sheet at $D = 30$ cm with (top) and without (bottom) a SF. Here the plastic substrate scatters light to angles larger than θ_{max} . Without a SF the off-axis photons scramble the useful information, reducing the image contrast. This phenomenon is a spatial-frequency-folding effect.

As was shown in this Letter, HH measures the field within the SF sampling cone without information loss. HH has many other advantages. By measuring the field in a $z = 0$ plane we are able to compute it at any z plane, thus getting three-dimensional information. Because the detected interference arises from the heterodyne mixing of a strong reference with a weak signal, HH is expected to be sensitive up to the photon level. Compared with intensity imaging, HH offers a huge dynamic range be-

References

1. D. Gabor. Microscopy by reconstructed wave-fronts. *Proceedings of the Royal Society of London. Series A, Mathematical and Physical Sciences*, pages 454–487, 1949.
2. T.M. Kreis, W.P.O. Jüptner, and J. Geldmacher. Principles of digital holographic interferometry. In *Proceedings of SPIE*, volume 3478, page 45, 1998.
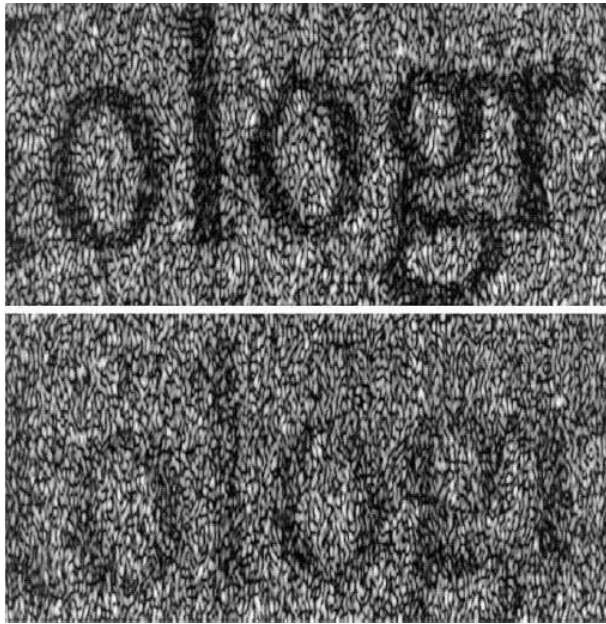
Fig. 5. Contact images of black characters printed on diffusive plastic sheets with (top) and without (bottom) a SF.

3. E. Cuche, P. Poscio, and C.D. Depeursinge. Numerical holography with digital recording devices. In *Proceedings of SPIE*, volume 3196, page 24, 1998.
4. E.N. Leith and J. Upatnnieks. Reconstructed wavefronts and communication theory. *J. Opt. Soc. Am.*, 52:1123–1128, 1962.
5. U. Schnars. Direct phase determination in hologram interferometry with use of digitally recorded holograms. *JOSA A*, 11(7):2011–2015, 1994.
6. U. Schnars, T.M. Kreis, and W.P.O. Jüptner. Digital recording and numerical reconstruction of holograms: reduction of the spatial frequency spectrum. *Optical Engineering*, 35:977, 1996.
7. M. Gross, F. Le Clerc, and L. Collo. *Waves and Imaging through complex media*, chapter Imagery of Diffusing Media by Heterodyne Holography. Kluwer Academic: P. Sebbah Ed., 2001.